A Novel Demodulator Design for Signal Processing of Inductive

Oil Debris Sensors

Guan Wang¹, Xianwei Wu ¹, Zhenghua Qian^{1,2}*, Dianzi Liu ³*, Peng Li^{1,2}, Iren Kuznetsova⁴

(1.Nanjing University of Aeronautics and Astronautics, State Key Laboratory of Mechanics and Control for Aerospace Structures, Nanjing, 210016;

2.Shenzhen Research Institute, Nanjing University of Aeronautics and Astronautics, Shenzhen, 518057, China

3. School of Engineering, University of East Anglia, Norwich, UK;

4. Nikov Institute of Radio Engineering and Electronics of RAS, Moscow 125009, Russia)

Abstract: Metal debris from bearing wear occurred in the lubrication system of aircraft engines represents valuable information, which can be utilized to assess the current engine condition and further enable the life-cycle prediction. The demodulation of debris signals consists of two parts: mixing and filtering. In traditional methods, the mixing process is complex to adjust and prone to failure, while the filtering employs the fixed low-pass filtering, which significantly affects the demodulation performance when the debris flow rate changes. To address these issues, this paper proposes a novel demodulation model to enhance the demodulation performance and increase the signal-to-noise ratio of chip signals. Firstly, the circuit innovatively adopts a self-frequency mixing method to avoid the complex phase adjustment required by traditional reference-frequency mixing methods for the improved stability of the circuit. Following that, a digital potentiometer is employed to implement the flow rate filtering, enabling precise control over the filter type and range, thus mitigating signal distortion caused by changes in flow rate and increasing the signal-to-noise ratio. Throughout extensive experiments and data analysis, the self-frequency mixing method improves the signal-to-noise ratio by 0.72 dB and reduces the signal standard deviation by 59.12% as compared to the reference-frequency mixing method. Considering the debris flow rate in the range of 0.2 to 0.5 m/s, the flow rate filtering method improves the signal-to-noise ratio by 19.71 dB and reduces the amplitude standard deviation by 66.18%, as compared to results by the traditional fixed low-pass filtering method. Results demonstrate that the aforementioned circuit design effectively enhances the signal amplitude and stability of inductive oil debris sensors in the wear assessment of mechanical systems and provides useful insights into the development of advanced sensors used in the field of structural health monitoring.

Keywords: Inductive oil debris sensor, Phase-lock-in amplifier, Digital potentiometer, Wave filter,

0.Introduction

The bearing component of aircraft engines operate at high speeds and under heavy loads, leading to the generation of metal debris due to wear[1, 2]. To reduce friction caused during bearing operation and prolong the bearing life, lubrication systems are designed for the bearings to mitigate the wear[3, 4]. The debris travels through the bearing in the lubrication system and is discharged after the filtration process[5]. Numerous studies have found that as the engine operates

^{*} Corresponding author

over time, the quantity and volume of metal debris generated by the bearings increase[6, 9]. Therefore, the condition of the bearings can be assessed by monitoring the quantity and size of debris in the lubricant, enabling the reliable engine life prediction[10, 12].

Considering the different physical properties of debris, research on oil debris monitoring has been conducted by various methods, including optical monitoring[13], radiographic monitoring[14], and electromagnetic monitoring[15], etc. Inductive oil debris sensors have advantages including the simple principle, small size, and clear signal mapping relationship, making them widely used in lubrication systems of large equipment such as aircraft engines and turbines[16, 17]. Early inductive debris sensors were single-coil structures proposed by Flanagan, consisting of a coil wound on a non-magnetic tube[18]. The coil, when energized, can detect changes in impedance within the tube, and the output signal from the coil is collected to determine the size of the debris in the signal amplitude analysis. In 2000, Miller et al. proposed a three-coil inductive debris sensor, which provides a stable magnetic field under static conditions using two opposing excitation coils and an induction coil placed in between [19]. This structure significantly improved the measurement accuracy and stability, capable of detecting 125µm debris in a 12mm diameter pipe. Ren et al. also improved the traditional three-coil structure using two semicircular induction coils. With a pipe diameter of 34mm, this sensor greatly enhances the accuracy of electromagnetic sensors and can detect ferromagnetic particles and non-ferromagnetic particles as small as 120um and 210um, respectively[20, 21].

The signal processing circuit of the sensor employs Phase-Lock-in Amplifier (PLA) technology to demodulate the signal. This method requires the mixture of a reference signal and the sensor signal before filtering to obtain the debris signal[22, 23]. However, this process encounters two main issues. Firstly, the reference signal needs to be in-phase and in-frequency with the sensor signal. This process involves an intricate phase adjustment. Moreover, variations in environmental temperatures can lead to changes in signal phase. Secondly, the low-pass filtering has to be used to remove the signal carrier wave in the filtering process. However, fixed filtering parameters cannot effectively filter signals from debris under different flow rates as the frequency of the debris signal is proportional to the oil flow rate.

1 Sensor and Circuit Introduction

1.1 Sensor Structure Overview

The sensor used in the experiment is a dual-exciter, single-inductive sensor. It consists of two excitation coils connected in parallel in opposite directions on both sides to generate a stable magnetic field. These coils have identical material properties, lengths, and coil interval. The induction coil is responsible for receiving the signal when the magnetic field changes within the sensor. It is wound around the center of the sensor without any external excitation. The structure diagram is shown in figure 1 below:

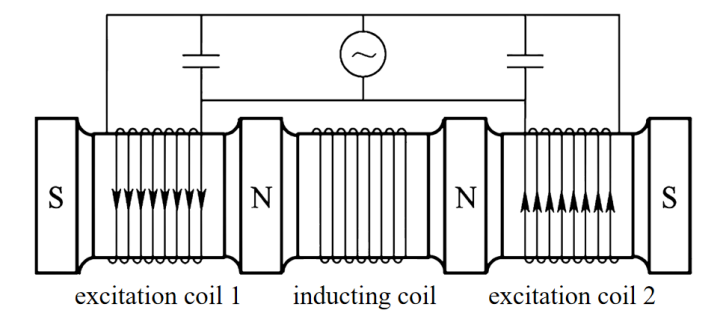


Figure. 1: Schematic Diagram of a Three-Coil Debris Sensor

When the sensor is in operation, the excitation source provides a high-frequency alternating current signal to the excitation coils, generating an alternating magnetic field around the coils. Since the two excitation coils form a symmetrical structure in opposite directions, the magnetic field intensity inside the pipe at any given time is symmetrically distributed if there is no debris passing through. As a result, the induced electromotive forces generated on the induction coil by the alternating magnetic field cancel each other out, and the induction coil does not produce any induction signal. However, when debris passes through, the internal magnetic field of the sensor changes, disrupting the magnetic field balance within the induction coil. This disruption causes the induction coil to generate an induced electromotive force, which is then received by the processing circuit. In this process, the excitation coils are subjected to a high-frequency alternating current signal with a frequency of several tens of kilohertz. When metal debris passes through the sensor, the signal received directly by the induction coil is an amplitude-modulated signal. The carrier frequency is the same as the excitation source frequency, while the modulated signal contains the debris information.

1.2 Introduction to conventional signal processing circuits

The sensor's complementary circuit consists of an excitation circuit and a signal processing circuit. In the excitation circuit, an STM32c8t6 chip is used to generate a sinusoidal signal with a frequency of 80 kHz. Amplified by a certain factor, this signal is then used as both the excitation signal and the reference signal for the sensor. The signal processing circuit is designed to demodulate the sensor signal. The schematic diagram of the required circuit is shown in figure 2 and its principles are described as follows:

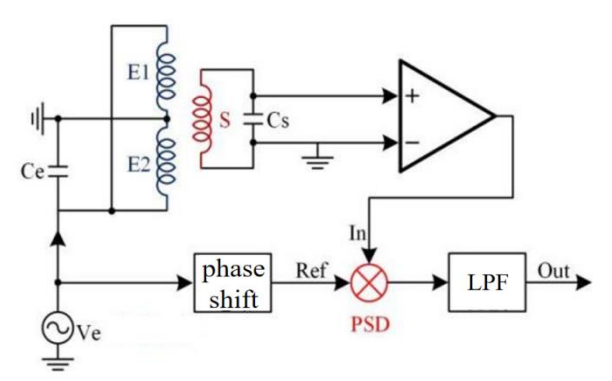


Figure. 2: Schematic Diagram of Signal Processing Circuit

- 1. The signal from the induction coil passes through a capacitor Cs for impedance matching, and then it is appropriately amplified by a certain factor using an amplifier to obtain the sensor signal.
- 2.A phase-shifting circuit is used to adjust the phase of the reference signal to be in phase with the sensor signal.
- 3. These two signals are then inputted into a PLA module aiming at frequency mixing.
- 4.A low-pass filter is utilized to remove the carrier wave and most of the noise for the extraction of the debris signal.

In the above process, mixing the reference signal with the sensor signal is termed as Reference Signal Mixing (RFM). The phase difference between the reference signal and the sensor signal is referred to as the mixing phase differences. Hence, the sensor signal can be formulated as:

$$u_s = a_s(t)\sin(2\pi f_c + \phi_c) \tag{1}$$

And the reference signal can be expressed as:

$$u_r = A_r \sin(2\pi f_c + \phi_r) \tag{2}$$

where as(t) represents the debris signal gain, f_c and φ_c denote the frequency and phase of the carrier wave, respectively. Ar stands for the amplitude of the reference signal, whose frequency is represented as φ_r .

Thus, the resulting signal is mathematically defined as:

$$u_{m1} = (1/2)a_s(t)A_r[\cos(\phi_c - \phi_r) - \cos(4\pi f_c + \phi_c + \phi_r)]$$
(3)

Finally, after low-pass filtering to remove high-frequency components, the expression for the debris signal obtained through RFM is expressed as:

$$u_{rfm} = (1/2)a_s(t)A_r\cos(\phi_c - \phi_r)$$
 (4)

It is noted that when the phase of the reference signal aligns with the phase of the sensor signal, the amplitude of the debris signal reaches its maximum value.

2.Improved Phase-Locked Amplifier

2.1 self-frequency mixing Circuit

To align the phase of the reference signal with that of the sensor signal, a phase-shifting circuit is designed for such adjustment. The schematic diagram of the circuit is shown in Figure 3:

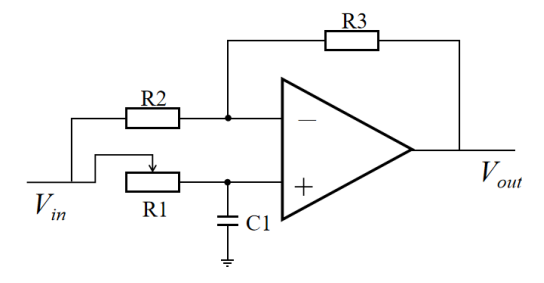


Figure. 3 Schematic Diagram of the Phase-Shifting Circuit

The above diagram depicts a common first-order phase-shifting circuit, which adjusts the phase of the input signal by varying the resistor R1. It is worth noting that the theoretical maximum phase shift is 90° and the effective adjustment range of the phase-shifting circuit is typically less than 60° in practical circuit applications. To achieve the precise in-phase alignment, it is necessary to connect multiple phase-shifting circuits in series for adjustment. This process is cumbersome, and variations in external temperature can induce the thermal drift in circuit components such as resistors and capacitors, causing phase deviation from the original phase shift and distorting output signals.

As the output signal varies significantly with phase differences between the reference signal and the measured signal, Signal Self-frequency mixing (SFM) is proposed to mitigate signal distortion caused by discrepancies in phase between the reference signal and the induced signal, thereby simplifying the operational complexity and enhancing detection accuracy. Moreover, SFM eliminates the need for phase adjustments even changes in sensor operating conditions are considered. This method circumvents the tedious process of phase adjustment and mitigates phase interference due to temperature drift. The schematic diagram of the circuit principle is illustrated

in figure 4:

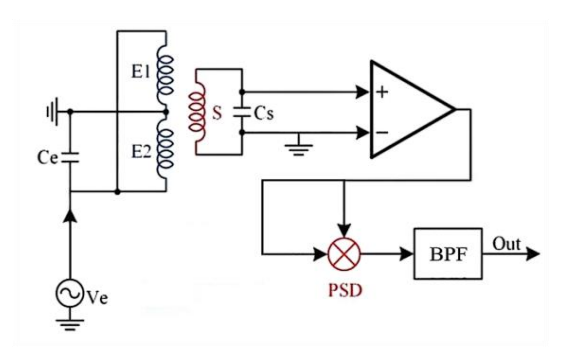


Figure. 4: Schematic Diagram of the SFM Circuit

With the implementation of SFM circuit, the improved debris signal processing can be divided into the following steps:

- 1.Amplify the signal obtained from the induction coil by an appropriate factor to obtain the sensor signal.
- 2. Split the sensor signal into two signals with the equal phase and amplitude.
- 3. Input the two signals into a phase-locked amplifier module for SFM.
- 4.Determine the main frequency of the debris signal through flow rate, allowing the single chip to determine the reasonable resistance value of the digital potentiometer.
- 5.Utilize a Butterworth band-pass filter to remove the carrier wave and most of the noise, extracting the debris signal.

The expression for the inputs of the mixer is defined as:

$$u_s = a_s(t)\sin(2\pi f_c + \varphi_c) \tag{5}$$

The expression for the SFM signal is:

$$u_{m2} = (1/2)a_s(t)A_r^2[1-\cos(4\pi f_c + 2\varphi_c)]$$
 (6)

Finally, after filtering out the high-frequency components, the expression for the debris signal obtained by the self-mixing is formulated as:

$$u_{sfm} = (1/2)a_s(t)A_r^2 (7)$$

It is noted that the amplitude of the SFM is independent of the signal phase.

2.2Flow rate filtering

The output signal from the mixer contains both high-frequency and low-frequency components. The low-frequency component, which represents the desired debris signal, needs to be separated from the surplus signals. Thus, it is essential to determine the appropriate filter bandwidth to eliminate unwanted signals.

The period of the signal generated by debris passing through the sensor can be approximated as the duration from entering one excitation coil to leaving the other, as illustrated in figure 5:

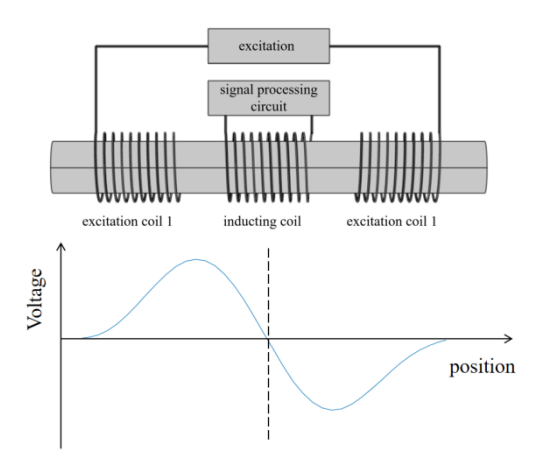


Figure. 5 Schematic diagram of debris signal cycle

When the velocity of debris is denoted at v and the length of the excitation coil is l, the center frequency f_0 of the debris signal can be expressed as v/l. From this equation, it's evidenced that the frequency of the debris signal is influenced by the flow rate. When the flow rate increases, the frequency of the debris signal also increases. If a low-pass filter is set at a fixed cutoff frequency, the filtering effectiveness may degrade or even fail when the flow rate changes. To address this issue, this paper proposes the use of a digital potentiometer and a single chip based Butterworth active band-pass filter. This filter adjusts the filtering range according to different flow rates, thus mitigating the effects of velocity variations on the filtering effectiveness. The filtering circuit is depicted in figure 6:

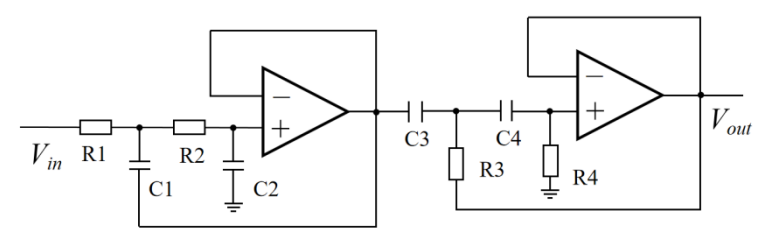


Figure. 6 Schematic diagram of active band-pass filtering

The proposed filtering circuit includes two operational amplifiers, capacitors and resistors, which constitute an active band-pass filter. The resistors are composed of two MCP42010 digital potentiometers, which are controlled by the single chip. Each digital potentiometer contains two adjustable resistors, with the resistance adjustment in the ranges of 0 to 10k, providing a total of 256 adjustment steps. Since this chip utilizes the SPI communication bus, multiple MCP42010 chips can be daisy-chained, allowing the single chip to control four resistors with a single command. The high-pass cutoff frequency of the filter is formulated as:

$$f_{cH} = \frac{1}{2\pi\sqrt{R_3R_4C_3C_4}} \tag{8}$$

And the low-pass cutoff frequency of the filter is determined by Eq.9:

$$f_{cL} = \frac{1}{2\pi\sqrt{R_1R_2C_1C_2}}$$
 (9)

In the actual circuit, fixed-value capacitors are selected and the bandwidth of the filter is

adjusted by varying the resistance of the digital potentiometer. Additionally, the use of digital potentiometer offers the advantage of accurately selecting resistor values to form optimized filters, such as Butterworth filters, Chebyshev filters, and Bessel filters. In this experiment, a Butterworth filter is employed, owing to its relatively flat frequency response within the pass-band and smooth transition between the pass-band and stop-band.

3 Introduction to experimental platform

3.1 Introduction to Signal Processing Circuits

The sensor utilized in this experiment is designed into a three-coil structure and its coils are wound around a ceramic frame. The coil assembly is housed within a metal casing, as depicted in figure 7:

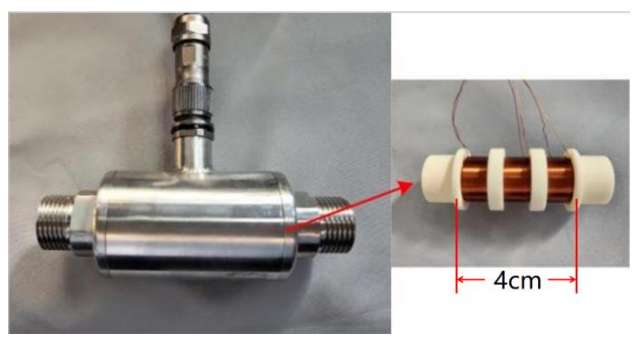


Figure.7 Schematic diagram of skeleton and Shell

The ceramic frame has an outer diameter of 14.5mm and an inner diameter of 13mm. Three coil slots with each width of 10mm, are engraved on the ceramic frame. These slots spaced 5mm apart from each other, are symmetrically centered. The induction coil is located at the central slot, while the two side slots accommodate the excitation coils. Using a winding machine, the copper wire with a diameter of 0.2mm is wound around the alumina ceramic frame. Each coil is wound with 6 layers, comprising 50 turns per layer. The excitation coils on both sides are wound in opposite directions. After completing the coil winding, the ceramic coil frame is placed into a stainless steel casing and securely fixed, with external wiring connections established.

3.2Introduction to the experimental platform

To assess the sensor quality and realize the movements of debris in the oil, an experimental platform is constructed as follows: Initially, the pre-made debris is fixed onto a transmission rope. Subsequently, the rope is driven by a motor to move, causing the debris to pass through the sensor. Finally, the signal output is received and stored by an oscilloscope. The schematic diagram and the apparatus of the experimental platform are shown in figure. 8 and figure 9, respectively:

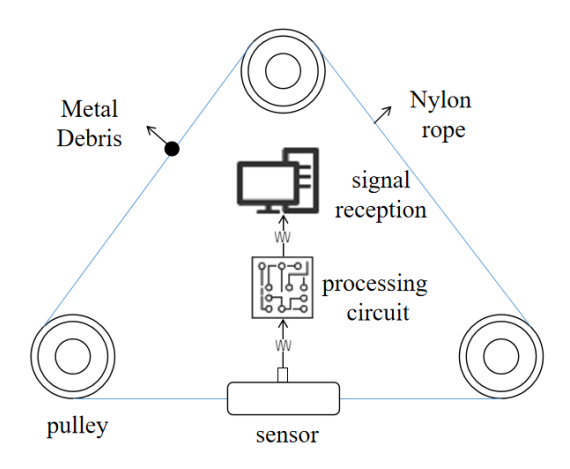


Fig.8 Schematic diagram of experimental testing platform

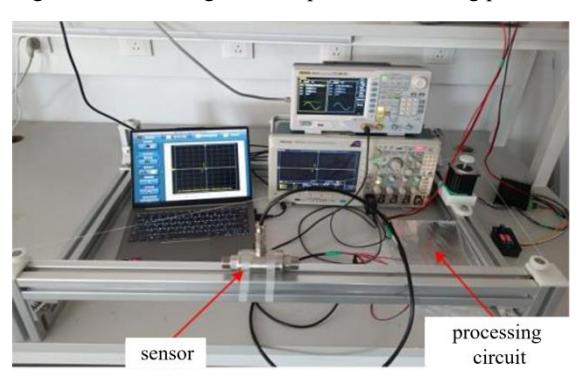


Figure.9 experimental and testing platform

The transmission rope is made of nylon material, whose magnetic permeability is close to that of air, thereby minimizing its impact on the internal magnetic field of the sensor. Furthermore, nylon rope exhibits excellent elasticity and moderate damping, making it less prone to sliding with the pulley during the rope transmission. The pre-made debris is chosen as spherical debris.

4 Experimental results and discussion

4.1 Comparison of mixed signals

With the proposed method, signals obtained from different mixing techniques are compared to demonstrate the stability of the SFM. Signals representing the information of 200 μ m debris are processed by various mixing methods with different mixing phase differences (0, $\pi/10$, $2\pi/10$, $3\pi/10$, and $4\pi/10$) are shown in figure 10. The debris velocity is 0.2m/s, and the filtering cutoff frequency ranges from 3.5-6.5Hz.

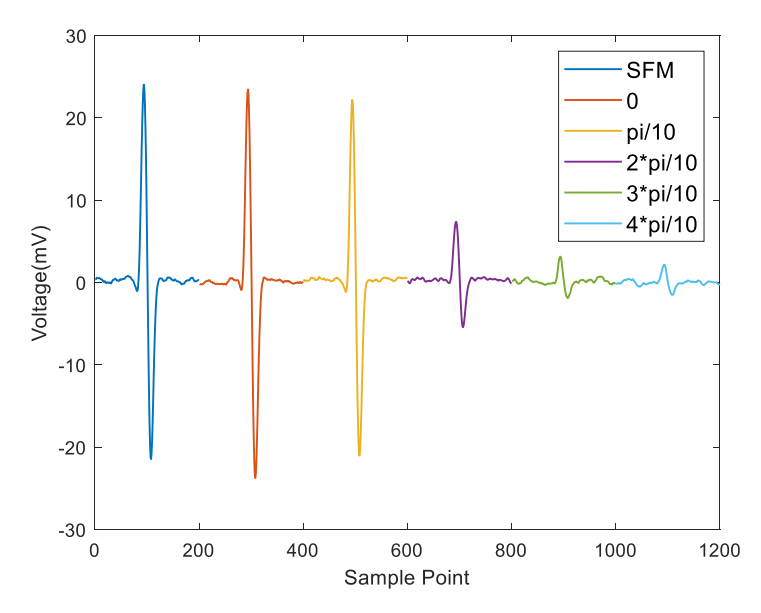


Figure. 10 Comparison of different mixing difference signals

It is noted that the amplitude of signals obtained by RFM gradually decreases as the mixing phase difference gradually increases. Each type of signal is collected twenty times, and the average signal-to-noise ratios are calculated as follows: 36.56dB, 32.15dB, 30.48dB, 21.83dB, 14.13dB, 13.93dB for the SFM signal and RFM signals with mixing phase differences of 0, $\pi/10$, $2\pi/10$, $3\pi/10$, $4\pi/10$, respectively. The signal-to-noise ratio of the SFM signal is slightly higher than that of the RFM signal. Moreover, as the SFM method does not require tedious manual adjustments, it can be better adapted to practical engineering requirements.

4.2 Diameter-amplitude mapping of SFM signals

Debris with diameters of 100, 150, 200, 250, and 300um are deliberately selected under a microscope. Signals are then collected 20 times for each debris size using both the RFM and SFM methods. Amplitude-diameter curves and standard deviation-diameter curves for the debris are provided in figure 11 and figure 12 throughout the statistical analysis. During the experiments, the debris velocity is set to 0.2m/s, and the filtering cutoff frequency varies in the range of 3.5 to 6.5Hz. A post-amplifier is employed to ensure that the average baseline noise measured in both mixing methods is controlled to 1 millivolt. The mixing phase difference of signals is adjusted to 0 in the RFM method.

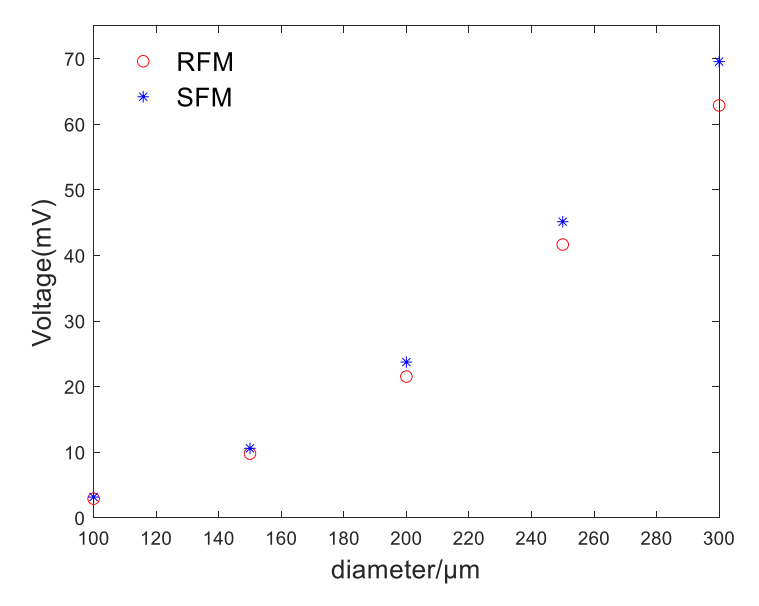


Figure. 11 Comparison of diameter-amplitude mappings

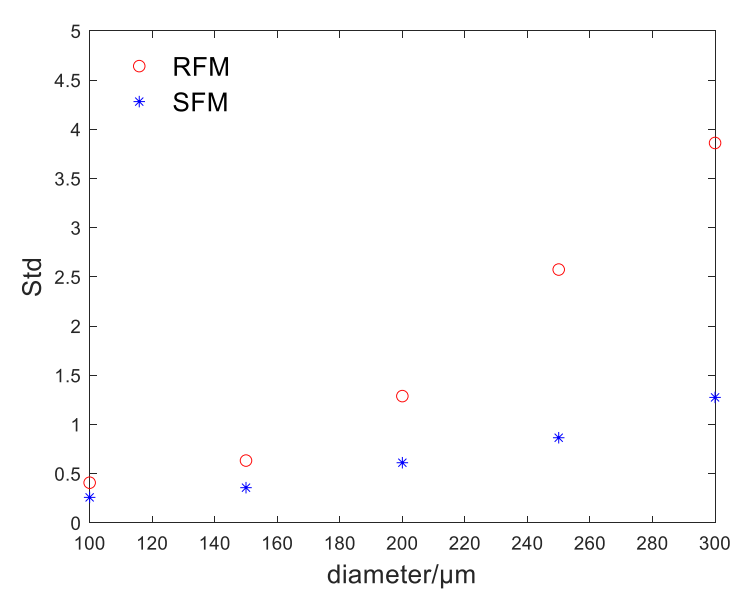


Figure. 12 Diameter-standard deviation comparison

In figure 11 and figure 12, it is evidenced that both signal amplitude and stability are improved using the SFM method. The statistical analysis reveals that the SFM method shows an average increase in amplitude of 0.72 dB, as compared to the RFM method. Furthermore, the standard deviation is also significantly reduced by 59.19%.

4.3 Analysis of flow rate filtering effects

At different flow rates, signals of 200um debris processed by fixed low-pass filters and digital variable band-pass filters are compared to demonstrate their superiority. Here, the SFM method is used for signal processing in all cases. Debris signals are collected under the flow rate filtering in the range of 0.2 m/s to 0.5 m/s with an increment of 0.05 m/s, and the corresponding center frequency is 5Hz-12.5Hz. Initially, the traditional low-pass filtering method uniformly sets the cutoff frequency to 16Hz, and signals obtained by traditional low-pass filters are investigated in figure 13. Then, signals are obtained using the flow rate filtering method, in which the band-pass filter bandwidth is set to the

center frequency of the debris signal with a tolerance of $\pm 30\%$, as shown in figure 14.

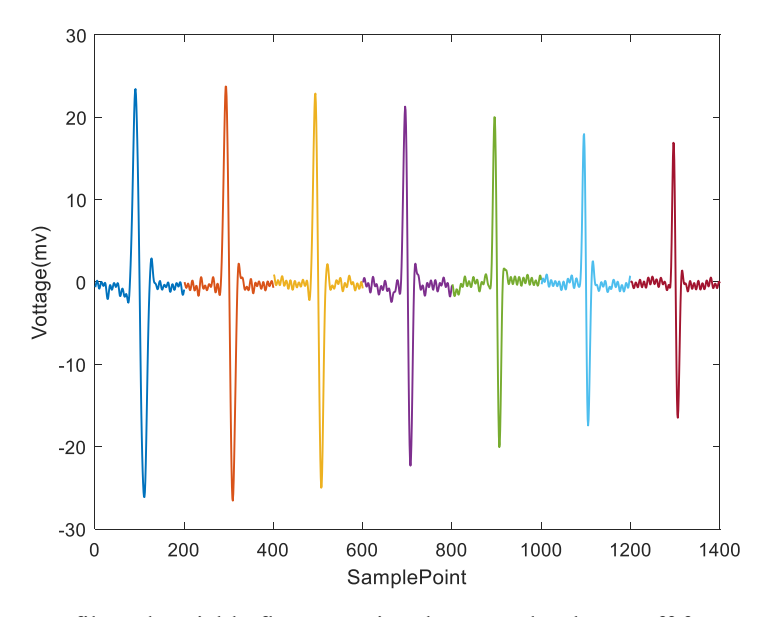


Figure. 13 Low-pass filtered variable flow rate signal map under the cutoff frequency of 16 Hz

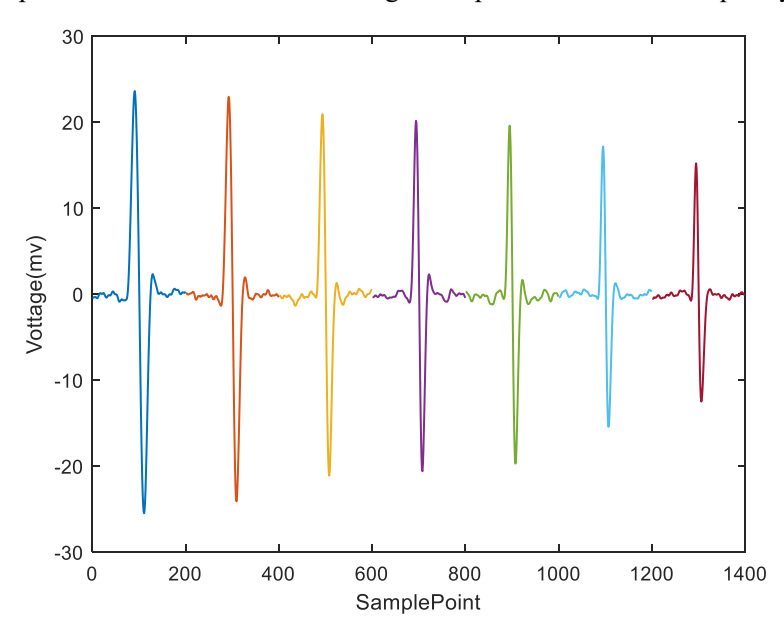


Figure. 14 Flow rate filtering signal map

In figure. 13 and figure 14, it is observed that the noise amplitude of the signal obtained by traditional low-pass filtering methods is relatively high, which is unfavorable for monitoring small-sized chips. However, after the same chip is filtered by the flow rate, the noise signal is significantly suppressed. Furthermore, as the frequency increases, the number of sampling points occupied by the debris signal gradually decreases, and the signal amplitude gradually diminishes. Due to the wide bandwidth feature of the filter, the signal contains a significant amount of noise, which severely affects the accurate identification of small debris particles.

For adjustable band-pass filtering, the bandwidth is narrower than that of traditional low-pass filtering. Consequently, the amplitude of the signal obtained through the flow rate filtering is slightly reduced and it almost maintains at the level of 20 voltage. Since the filter bandwidth encompasses the central frequency of the debris signal and is within a reasonable range, the

signal-to-noise ratio of the debris signal becomes larger, and the amplitude of the debris signal remains relatively stable. This stability is extremely beneficial to the size analysis of debris particles. Throughout twenty experiments for statistical analysis, the debris signal amplitudes are shown in Table 1. It is worth noting that when the debris flow rates range from 0.2 to 0.5 m/s, the signal-to-noise ratio of flow rate filtering is averagely increased by 19.71 dB and the standard deviation of the debris signal is reduced by 66.18%, as compared with results by the low-pass filtering. This demonstrates both the signal-to-noise ratio and signal stability are significantly improved by the proposed circuit design.

	flow rate(m/s)		0.2	0.25	0.3	0.35	0.4	0.45	0.5
•	low-pass	SNR(dB)	21.05	21.17	20.85	20.22	19.69	18.75	18.22
	filtering	Std (mV)	0.41	0.43	0.85	0.74	0.52	0.48	0.68
	flow rate	SNR(dB)	38.13	37.53	36.41	37.48	36.72	35.71	36.24

0.30

0.53

0.23

0.48

0.38

0.39

0.41

Table 1 Comparison table of filtered amplitude

5. Conclusion

filtering

Std (mV)

To address two grand challenges arising from the post-processing of signals by inductive debris sensors, the Self-frequency mixing method (SFM) is proposed to simplify the circuit testing process, enhancing the stability of the mixing process. Meanwhile, a flow rate filtering method is introduced to precisely control the type and range of filtering, thereby increasing the signal-to-noise ratio of the debris signal. The feasibility of the proposed design is validated throughout experimental comparisons. Results indicate that SFM improves the signal-to-noise ratio by 0.72 dB and reduces the signal standard deviation by 59.12% as compared to the traditional method. Considering the debris flow rates in the range of 0.2 to 0.5 m/s, the flow rate filtering method improves the signal-to-noise ratio by 19.71 dB and reduces the amplitude standard deviation by 66.18% in comparison of the results by the traditional fixed low-pass filtering method. Summarily, the significance of this study is highlighted by its practical application for the realization of signal demodulation with the improved stability and signal-to-noise ratio, and also provides a new approach for the monitoring of debris in aviation engines and related equipment, laying a solid foundation for the health monitoring of aviation engines.

CRediT authorship contribution statement

Guan Wang: Conceptualization, Methodology, Writing-original draft .Xianwei Wu: Methodology, Investigation, Validation. Dianzi Liu: Supervision, Reviewing and Editing.

Declaration of Competing Interest

The authors declare that they have no known competing financial interests or personal relationships that could have appeared to influence the work reported in this paper.

Acknowledgement

This work was supported by the National Key Research and Development Program of China (2023YFE0111000), National Natural Science Foundation of China (12172171, 12372151), National Natural Science Foundation of Jiangsu Province (BK20211176), and Shenzhen Science and Technology

References

- [1] Y. Xie, Y. Zhang, H. Zhang, H. Shi, D. Wu, S. Zhang, Y. Sun, Design of a micro-triple-coil multi-pollutant detection sensor based on high-gradient magnetic field, Sensors and Actuators A: Physical, 362 (2023).
- [2] N.H. Harun, N. Misron, R.M. Sidek, I. Aris, D. Ahmad, H. Wakiwaka, K. Tashiro, Investigations on a novel inductive concept frequency technique for the grading of oil palm fresh fruit bunches, Sensors (Switzerland), 13 (2013) 2254-2266.
- [3] X. Wu, Y. Zhang, N. Li, Z. Qian, D. Liu, Z. Qian, C. Zhang, A new inductive debris sensor based on dual-excitation coils and dual-sensing coils for online debris monitoring, Sensors, 21 (2021).
- [4] A. Regis, J.M. Linares, S. Arroyave-Tobon, E. Mermoz, Numerical model to predict wear of dynamically loaded plain bearings, Wear, 508-509 (2022).
- [5] Hong W, Wang S, Tomovic MM, et al. A new debris sensor based on dual excitation sources for online debris monitoring[J]. Measurement Science and Technology, 2015, 26(9).
- [6] T. Liu, H. Sheng, Z. Jin, L. Ding, Q. Chen, R. Huang, S. Liu, J. Li, B. Yin, A High-Confidence Intelligent Measurement Method for Aero-Engine Oil Debris Based on Improved Variational Mode Decomposition Denoising, Aerospace, 10 (2023).
- [7] X. Wu, H. Liu, Z. Qian, Z. Qian, D. Liu, K. Li, G. Wang, On the Investigation of Frequency Characteristics of a Novel Inductive Debris Sensor, Micromachines, 14 (2023).
- [8] R.D. Nugraha, S. Chen, N. Yin, T. Wu, Z. Zhang, Running-in real-time wear generation under vary working condition based on Gaussian process regression approximation, Measurement: Journal of the International Measurement Confederation, 181 (2021).
- [9] Qian M, Ren Y, Feng Z. Interference reducing by low voltage excitation for a debris sensor with triple-coil structure[J]. Measurement Science and Technology, 2019, 31(2).
- [10] J. Guo, S. Huang, R. Wu, T. Ye, Z. Chen, A method to calculate the life of sliding bearings based on fatigue and wear failure considering fluid lubrication, Journal of Physics: Conference Series, 2020.
- [11] P. Wang, D. Li, N. Zhang, Research on early warning of rolling bearing wear failure based on empirical mode decomposition, International Journal of Materials and Product Technology, 63 (2021) 72-85.
- [12] Y. Wu, H. Zhang, Solid particles, water drops and air bubbles detection in lubricating oil using microfluidic inductance and capacitance measurements, Journal of Micromechanics and Microengineering, 29 (2019).
- [13] T. Wang, Y. Guo, G. Wang, X. Wang, Detection and analysis of metal scrap in lubricating oil based on wear fault of spindle bearing of turboshaft engine, Vibroengineering Procedia, 2021, pp. 32-37.
- [14] B. Yu, N. Cao, T. Zhang, A novel signature extracting approach for inductive oil debris sensors based on symplectic geometry mode decomposition, Measurement: Journal of the International Measurement Confederation, 185 (2021).
- [15] Z. Liu, Y. Liu, H. Zuo, H. Wang, C. Wang, Oil debris and viscosity monitoring using optical measurement based on Response Surface Methodology, Measurement: Journal of the International Measurement Confederation, 195 (2022).

- [16] Z. Duan, T. Wu, S. Guo, T. Shao, R. Malekian, Z. Li, Development and trend of condition monitoring and fault diagnosis of multi-sensors information fusion for rolling bearings: a review, International Journal of Advanced Manufacturing Technology, 96 (2018) 803-819.
- [17] J. Zhe, X. Zhu, C. Zhong, A high sensitivity wear debris sensor using ferrite cores for online oil condition monitoring, Measurement Science and Technology, 28 (2017).
- [18] I.M. Flanagan, J.R. Jordan, H.W. Whittington, An inductive method for estimating the composition and size of metal particles, Measurement Science and Technology, 1 (1990) 381-384.
- [19] J.L. Miller, D. Kitaljevich, In-line oil debris monitor for aircraft engine condition assessment, IEEE Aerospace Conference Proceedings, 6 (2000) 49-56.
- [20] Y.J. Ren, W. Li, G.F. Zhao, Z.H. Feng, Inductive debris sensor using one energizing coil with multiple sensing coils for sensitivity improvement and high throughput, Tribology International, 128 (2018) 96-103.
- [21] Y.J. Ren, S.W. Gao, X.L. Wen, Y.B. Liu, B. Ju, The research on triple-coil inductive debris sensor with electromagnetic shielding, Measurement Science and Technology, 35 (2024).
- [22] X. He, Y. Li, Z. Meng, L. Lin, D. Chen, M.S. Zhang, Z. Wang, A novel TMR sensor based on digital lock-in amplifier technology for portable oil multipollutant detection system, Sensors and Actuators A: Physical, 369 (2024).
- [23] Y.J. Ren, G.F. Zhao, M. Qian, Z.H. Feng, A highly sensitive triple-coil inductive debris sensor based on an effective unbalance compensation circuit, Measurement Science and Technology, 30 (2019).